



LAWRENCE  
LIVERMORE  
NATIONAL  
LABORATORY

# Design of Short Pulse Laser Driven Opacity Experiments

R. A. London, J. I. Castor

July 15, 2013

High Energy Density Physics

## **Disclaimer**

---

This document was prepared as an account of work sponsored by an agency of the United States government. Neither the United States government nor Lawrence Livermore National Security, LLC, nor any of their employees makes any warranty, expressed or implied, or assumes any legal liability or responsibility for the accuracy, completeness, or usefulness of any information, apparatus, product, or process disclosed, or represents that its use would not infringe privately owned rights. Reference herein to any specific commercial product, process, or service by trade name, trademark, manufacturer, or otherwise does not necessarily constitute or imply its endorsement, recommendation, or favoring by the United States government or Lawrence Livermore National Security, LLC. The views and opinions of authors expressed herein do not necessarily state or reflect those of the United States government or Lawrence Livermore National Security, LLC, and shall not be used for advertising or product endorsement purposes.

# Design of Short Pulse Laser Driven Opacity Experiments

R. A. London\* and J. I. Castor

Lawrence Livermore National Laboratory, Livermore, California, 94550

## ABSTRACT

Hot electrons created by short, intense laser pulses can heat solid density material to temperatures of order 500 eV. Inertial confinement can maintain such hot-dense plasmas for times of order 10 ps. This provides a platform for measurement of basic properties of hot dense matter, such as opacity and equation-of-state. In this paper we describe the role of computational modeling in the design and analysis of such opacity experiments. We describe a method to model the hot electron transport and deposition and the resulting target radiation-hydrodynamics. We present several design concepts to achieve uniform, long-lasting plasmas.

## 1. Introduction

The measurement of radiative opacities relevant to stellar physics and inertial confinement fusion has been pursued for a number of years. Most prior research has used long-pulse lasers, e.g. [1,2] and Z-pinch machines, e.g. [3] to obtain opacities of materials with temperatures between 15 and 150 eV and densities in the range  $10^{21}$ - $10^{23}$  electrons/cm<sup>3</sup>. A review of these long-pulse techniques is given by Bailey, et al. [4].

During this same period, it has been recognized that high intensity, short pulse lasers (in the ps regime) can be used to heat solid targets to temperatures in the range of 100 to 500 eV. Early work relied on heating by laser absorption and thermal electron conduction of surface or near-surface layers, e.g. [5-8]. Later work utilized deep heating by supra-thermal (“hot”) electrons, generated by anomalous absorption of the laser light [9-12, and references therein]. Measurements of the temperatures of short pulse heated buried layers versus target thickness and laser intensity and wavelength have been presented by Brown, et al. [13]. It has been found that a large fraction of the energy in a short, high-intensity optical laser pulse can be converted into hot electron energy at the surface of a solid target [14, 15, and references therein]. Laser pulses with durations of

---

\* Corresponding author. Tel: 925 253 1467  
E-mail address: [rlondon@llnl.gov](mailto:rlondon@llnl.gov) (R. A. London)

order 1 ps and intensities of order  $10^{19}$  W/cm<sup>2</sup> produce electrons with energies in the 100 keV-MeV range [16]. The hot electrons propagate tens to hundreds of microns into a target, where they heat the bulk material. Due to the rapid heating, plasmas can be created with densities equal to the initial (solid) value, of order 1-20 g/cc and temperatures of order 500 eV. This enables the creation of hot dense matter at controlled conditions and allows the measurement of properties such as the equation-of-state and opacity of the material.

The use of short-pulse lasers for measuring opacity has been proposed [17,18] and preliminary experiments have been carried out [19]. The short pulse optical laser heating method allows the study several important opacity processes such as atomic models, continuum lowering, and line broadening. This is important for applications such as inertial confinement fusion and for modeling of stellar structure and evolution. It will also enable the study of high-temperature radiation-hydrodynamics phenomena, such as radiative collapse.

## 2. Experimental Concept

A schematic picture of an experiment to determine opacity by measuring the emission from an ultra-short-pulse (USP) heated target is illustrated in Figure 1 [19]. A specific target design comprises a light-element “tamper” foil containing a thin buried layer, which is irradiated on one side by a short laser pulse. Hot electrons generated at the surface stream through and heat the bulk of the target, including the buried layer. The x-ray emission from the layer is measured with a time resolved spectrometer. In addition, the spectra of reference ions, such as H- and He-like ions, are measured and fit to calculations to give the temperature and density of the layer versus time. The frequency dependent opacity  $\kappa_\nu$  can be expressed in terms of the specific intensity emergent from the target ( $I_\nu$ ) by solving the radiation transfer equation for a thin slab of thickness  $\Delta z$ :

$$\kappa_\nu = \frac{-\ln [1 - I_\nu / B_\nu(T)]}{\Delta z},$$

where  $B_\nu(T)$  is the Planck function and we have assumed local thermodynamic equilibrium (LTE). The intensity is determined from the measured signal strength (power/frequency), knowing the emission area of the target and the angular acceptance and efficiency of the spectrometer.

The design of a target for opacity measurements must consider several goals, such

as achieving the desired temperature and density, achieving uniformity in these conditions in space and time, achieving LTE or near-LTE conditions, and producing sufficient x-ray emission to record high signal-to-noise spectra. Parameters such as the composition, structure, and size of the target and the wavelength, energy, duration, and focal spot size of the laser pulses are to be chosen to achieve the design goals. We describe the design of such experiments utilizing computational modeling.

### 3. Simulation methodology

We use the LASNEX radiation-hydrodynamics computer program to model the target dynamics [20, 21]. Initially developed to model laser inertial confinement fusion, LASNEX includes models for laser propagation, compressible hydrodynamics, atomic ionization and excitation, heat conduction and radiation transport, among other processes. All of these models are coupled together to allow time-dependent simulations of laser-heated targets. Most importantly for this work, LASNEX contains a model for the transport and coupling of supra-thermal or hot electrons [22]. The hot electrons are treated by a multi-group diffusion model, which accounts for self-consistent electric fields, assuming quasi-neutrality. This includes a cold return current that balances the current of hot electrons flowing out of the source region. The velocity is assumed to be isotropic, to first order, with the drift velocity small compared to the thermal velocities. There are no magnetic fields and reflecting boundary conditions are imposed, meaning that the escape of electrons from the target is not allowed. This assumption is justified by estimating the escape fraction with a capacitor model [23,24]. Energy is coupled from the hot electrons to the cold matter by three processes: Coulomb collisions between hot and cold electrons, resistive heating due to the cold return current (also known as “ $\mathbf{J}\cdot\mathbf{E}$ ” heating), and hot-electron pressure gradient (“PdV”) work. The other physics models we use are an average atom model for atomic physics, flux-limited electron heat conduction, Lagrangian hydrodynamics, and multi-group diffusion x-ray transport.

The work presented here assumes one-dimensional plane-parallel symmetry. This is expected to be a reasonable approximation for the hydrodynamic and radiative properties of the thin buried layer for which we want to measure the opacity. However, it does not account for lateral transport of hot electrons. The LASNEX-based model is not very accurate for such transport due to its lack of angularly resolved transport and magnetic fields. We therefore stick with one-dimensional calculations and adjust the input power of hot electrons to account for both the uncertain laser conversion efficiency and lateral transport of the hot electrons.

To model short-laser-pulse heated targets, we assume that a fraction of the laser energy is transferred to hot electrons, placed in a thin region (0.1  $\mu\text{m}$ -thick) at the surface of the target with a temporal pulse equal to that of the laser pulse. The fraction is based on past experiments and particle-in-cell simulations [15]. We assume that the initial energy distribution is Maxwellian [14,25]. The simulation is thus driven by the transport of the hot electrons and their energy and momentum coupling to the cold matter.

#### 4. Simulation Results

We first present results from a target containing an Al buried layer similar to the targets described in ref. [13]. The target has a 0.15- $\mu\text{m}$ -thick layer of Al, with 6  $\mu\text{m}$  of plastic (“CH”) on the front and 2  $\mu\text{m}$  on the back. We input a 0.5 ps flattop pulse of hot electrons with a temperature of 300 keV and an intensity of  $3.8 \times 10^{17} \text{ W/cm}^2$ . This intensity, which is approximately 4% of the laser intensity in the experiments, was chosen to match the temperatures inferred in the experiments. This percentage represents both the conversion efficiency of laser light to hot electron energy and a loss due to lateral transport. We typically simulate 20 ps of time, utilizing 300 spatial zones and 4,000 time-steps. Simulations take 10-60 minutes on single processor computers. In this simulation nearly all of the hot electron energy is coupled to the target in 20 ps. Approximately 59% goes into PdV coupling, mainly on the outer layers of the target, 36% is coupled to the thermal electrons by collisions and 5% by resistive heating. About 6% of the coupled energy is lost by radiative cooling.

Figure 2 shows the time and space dependence of the electron temperature and the mass density of the target. The hot electrons are injected at the right side of the panels, at  $z=8 \mu\text{m}$ . Figure 2a shows a build-up to maximum temperature in about 4 ps and a spatial gradient from the front to the back of the target (right to left). The Al layer, which starts out at 2  $\mu\text{m}$ , remains slightly cooler than the surrounding CH, due to radiative cooling. The temperature within the layer is nearly uniform. The density plot in 2b shows an early expansion of the Al followed by a period of fairly constant density. We also see rarefaction waves traveling inward from the surfaces of the CH. The rarefaction from the rear surface ( $Z=0$ ) reaches the Al layer at 10 ps. After that time, the layer begins to expand and move towards the left, pushed by the pressure gradient, which is related to the temperature gradient.

The time variation of the temperature and density at the center of the Al layer are shown in Figure 3. The conditions are nearly constant between 2 and 12 ps, with  $T_e = 510 \pm 50 \text{ eV}$  and  $\rho = 1.8 \pm 0.2 \text{ g/cc}$ . This temperature is within the range measured using

similar targets at the HELEN laser [13]. This target provides a 10-ps-long period with constant and uniform high-temperature-high density plasma conditions, during which opacity could be measured.

Several target concepts can be invoked to achieve different densities and temperatures. The temperature can be adjusted by varying the irradiance—within the constraints of laser system available. The density can be varied by using a higher density tamper material and/or by using a long pulse laser to pre-compress the target. Figure 4 shows the evolution of the layer conditions for 3 different tamper materials, CH, amorphous carbon (aC), and diamond, with densities of 1.1, 2.0 and 3.5 g/cc, respectively. The CH tamper was the same thickness as for the case considered in Figs. 2 and 3, but the Al layer was placed in the center of the target rather than towards the back. The targets with the other tamper materials have the same mass column density ( $\rho\Delta z$ ) and are therefore thinner than the CH target. The density of the layer during the stationary period increases with increasing tamper density (panel a), while the peak temperature is relatively constant (panel b). The increased density is accompanied by a shorter stationary period, before the layer decompresses.

We can also increase the density by using a long pulse laser to irradiate the back of the target and drive a shock wave through it [19]. A simulation has been done using a 200-ps long flattop pulse at an intensity of  $6 \times 10^{14}$  W/cm<sup>2</sup> irradiating a 14- $\mu$ m thick diamond target containing a 0.15- $\mu$ m Al layer located 4  $\mu$ m from the front side. At the end of the long pulse, a short 0.5 ps hot electron pulse is imposed at the front side, as in the previous example. The target evolution is shown in Figure 5. The long pulse laser drives a shock through the diamond at a speed of about 55  $\mu$ m/ns. The shock compresses the diamond by a factor of about 3.3 to a density of 11.5 g/cc (panel a). The shock raises the temperature to about 20 eV. The shock then hits the Al layer at 180 ps, compressing it to 12 g/cc. We turn on the short pulse at 200 ps and achieve a temperature of 550 eV (not shown in the figure). Further simulations show that we can achieve lower densities by lower the long pulse laser intensity. For example, with an intensity of  $2 \times 10^{13}$  W/cm<sup>2</sup>, we get a density of 7 g/cc. The shock velocity is smaller so that a longer period must be allowed between the long and short pulses—800 ps in this example. By invoking the two methods just described, one can achieve densities between 1.8 and 12 g/cc in an Al buried layer.

## 5. Stellar Opacity Experiment

Opacity is a key property determining the structure and evolution of the sun and

similar stars. Our understanding of stars relies heavily on computational models, which in turn rely on theoretical opacities. It is fundamental to check the accuracy of these opacities with direct experimental measurements. There is currently particular interest in the upper region of the radiative zone of the sun, extending up to the boundary with the convective zone. This region has temperatures between 150 and 400 eV and electron densities between  $10^{23}$  and  $10^{24}$   $\text{cm}^{-3}$ , as shown in Figure 6 [26]. There is currently a disagreement between model predictions and helio-seismic observations, which could be reconciled if the Rosseland mean opacities were approximately 10-20% larger than the theoretically calculated values [27]. The main elements of interest are oxygen, which is responsible for ~35% of the opacity at the boundary, and iron, which contributes up to 20% in the radiative zone. Iron is a prime candidate for experimental study due to its large contribution and its complex spectrum, which is difficult to calculate. Several groups have proposed and/or performed experiments on stellar opacity, as reviewed in refs. [4, 28]. A recent paper proposes an experiment using the long-pulse NIF laser [29].

We propose a short-pulse laser experiment to measure stellar opacity. To access conditions appropriate to the radiative region of the sun, we propose a CH tamped target similar to those discussed above. The first design assumes a 0.1  $\mu\text{m}$  Fe layer at the center of a 9  $\mu\text{m}$ -thick CH tamper. In order to achieve a temperature of around 300 eV, the hot electron intensity in a 1D simulation is  $2.4 \times 10^{17}$   $\text{W}/\text{cm}^2$ , 40% lower than in the previous examples. Based on the experimental results of ref. [13], we estimate that this could be obtained with 0.53  $\mu\text{m}$  laser light at an intensity of approximately  $5 \times 10^{18}$   $\text{W}/\text{cm}^2$ . Simulated temperature and electron density histories are shown in Figure 7. The Fe layer behaves somewhat differently from the Al layer discussed previously. The electron density initially increases as the layer gets heated up and ionized during the first ps (Fig. 7a). Then the iron layer expands for a few ps, since its density is much higher than the surrounding CH. This is followed by a period when the density increases from 4 to  $6 \times 10^{23}$   $\text{cm}^{-3}$  between 3 and 23 ps, accompanied by a decreasing temperature from 260 to 200 eV. This response is governed by radiative cooling. About 11% of input hot electron energy is radiated in this case. Since the iron radiates more effectively than the surrounding CH, its temperature drops below that of the CH. This causes a pressure gradient, which compresses the layer. This radiative cooling and collapse period ends when rarefaction waves from the target surfaces reach the center and the layer expands and cools rapidly after 23 ps.

The specific intensity emitted by the Fe buried layer target at a time of 5 ps, near peak emission, is shown in Figure 8. The spectral calculation uses the DCA (detailed configuration accounting) atomic model within Lasnex [30, 31]. This model includes

multiple ionization stages and angular momentum splitting of the principal quantum shells and therefore produces a more detailed spectrum than the average atom model. The spectrum is dominated by L-shell emission of  $\text{Fe}^{+16} - \text{Fe}^{+19}$  in the region between 0.8 and 1.1 keV. The rising emission towards lower energy is mainly from the CH tamper foil. The emission lasts approximately 20 ps. The intensity level of around  $6 \times 10^{13} \text{ W/keV/cm}^2/\text{sr}$  is somewhat smaller than the L-shell intensity measured from Ge targets at the HELEN laser [19] and is expected to be detectable with sensitive spectrometers.

An alternate target design enables one to obtain somewhat lower and more constant density conditions. This is accomplished by using a layer with a mixture of Fe and CH. We have performed simulations for layers with 10% and 20% atomic concentration of Fe, again at the center of an 9  $\mu\text{m}$ , pure CH foil. The thickness of the layer is chosen to maintain the same amount of Fe. The density is specified by adding the concentration-weighted specific volumes of the solid materials. Thus the 10% layer has a density of 1.52 g/cc and a thickness of 1.59  $\mu\text{m}$ . The results of simulations for targets with 10 and 20% Fe are shown in Figure 7. The 10% target shows a 20 ps period in which the density is nearly constant at  $4 \times 10^{23} (\pm 10\%)$ , while the temperature varies from 290 to 210 eV. The experimental fielding of buried Fe layer targets should allow the measurement of opacity in an important spectral region for stellar modeling

## 6. Conclusions

We have presented numerical simulations of thin buried layer targets heated by hot electrons generated by high intensity short laser pulses. We have found that layers of order 0.1  $\mu\text{m}$  in foils several  $\mu\text{m}$  in thickness can be heated to temperatures of approximately 500 eV at densities near the original solid value, in agreement with recent experiments. We show that alternate tamper materials can produce buried layers of different densities. The use of a long pulse irradiating one side of the target produces a shock wave, which pre-compresses the target and leads to a higher density layer that can be heated by a short pulse incident on the other side of the target. Finally, we propose that opacities relevant to the solar interior can be measurement by x-ray emission from a short pulse heated target

## Acknowledgements

We thank M. Tabak, G. Zimmerman, J. Nilsen for discussions of short-pulse

laser-target modeling techniques, C. Iglesias and B. Wilson for discussions of the role of opacity in stellar and ICF systems, R. Shepherd, J. Dunn, P. Beiersdorfer and A. Steele for discussions of experimental concepts. This work was performed under the auspices of the U.S. Department of Energy by Lawrence Livermore National Laboratory under Contract DE-AC52-07NA27344

## References

- [1] S. J. Davidson, J. M. Foster, C. C. Smith, K. A. Warburton, and S. J. Rose, Investigation of the opacity of hot, dense aluminum in the region of its K edge, *App. Phys. Lett.*, 52 (1988) 847-849.
- [2] P. T. Springer, D. J. Fields, B. G. Wilson, J. K. Nash, W. H. Goldstein, C. A. Iglesias, F. J. Rogers, J. K. Swenson, M. H. Chen, A. Bar-Shalom, and R. E. Stewart, Spectroscopic absorption measurements of an iron plasma, *Phys. Rev. Lett.* 69 (1992) 3735–3738.
- [3] J. E. Bailey, G. A. Rochau, C. A. Iglesias, J. Abdallah, Jr., J. J. MacFarlane, I. Golovkin, P. Wang, R. C. Mancini, P. W. Lake, T. C. Moore, M. Bump, O. Garcia, and S. Mazevet, Iron-plasma transmission measurements at temperatures above 150 eV, *Phys. Rev. Lett.*, 99 (2007) 265002-1-4.
- [4] J. E. Bailey, G. A. Rochau, R. C. Mancini, C. A. Iglesias, J. J. MacFarlane, I. E. Golovkin, C. Blancard, Ph. Cosse, and G. Faussurier, Experimental investigation of opacity models for stellar interior, inertial fusion, and high energy density plasmas, *Phys. Plasmas*, 16 (2009) 058101-1-16.
- [5] M. M. Murnane, H. C. Kapteyn, and R. W. Falcone, High-density plasmas produced by ultrafast laser pulses, *Phys. Rev. Lett.*, 62 (1989) 155-158.
- [6] K. Nazir, S. J. Rose, A. Djaoui, G. J. Tallents and M. G. Holden, P. A. Norreys, P. Fewes, J. Zhang, and F. Failles, X-ray spectroscopic studies of hot, dense iron plasma formed by subpicosecond high intensity KrF laser irradiation, *Appl. Phys. Lett.*, 69, (1996) 3686.
- [7] G. Guethlein, M. E. Foord, and D. Price, Electron temperature measurements of solid density plasmas produced by intense ultrashort laser pulses, *Phys. Rev. Lett.*, 77 (1996) 1055-1058.
- [8] B. K. F. Young, B. G. Wilson, G. B. Zimmerman, D. F. Price, R. E. Stewart, Generation and modeling of near-LTE plasmas using ultrashort pulse laser heated, tamped mid-Z targets, *J. Quant. Spectrosc. Radiat. Transf.* , 58 (1997) 991-1000.
- [9] J. A. Koch, M. H. Key, R. R. Freeman, S. P. Hatchett, R. W. Lee, D. Pennington, R. B. Stephens, and M. Tabak, Experimental measurements of deep directional columnar

heating by laser-generated relativistic electrons at near-solid density, *Phys. Rev. E*, 65 (2001) 016410.

[10] G. Gregori, S. B. Hansen, R. Clarke, R. Heathcote, M. H. Key, J. King, R. I. Klein, N. Izumi, A. J. Mackinnon, S. J. Moon, H.-S. Park, J. Pasley, N. Patel, P. K. Patel, B. A. Remington, D. D. Ryutov, R. Shepherd, R. A. Snavely, S. C. Wilks, B. B. Zhang, S. H. Glenzer, Experimental characterization of a strongly coupled solid density plasma generated in a short-pulse laser target interaction, *Contrib. Plasma Phys.*, 45 (2005), 284–292.

[11] D. J. Hoarty, S. F. James, H. Davies, C. R. D. Brown, J. W. O. Harris, C. C. Smith, S. J. Davidson, E. Kerswill, B. J. B. Crowley, and S. J. Rose, Heating of buried layer targets by  $1\omega$  and  $2\omega$  pulses using the HELEN CPA laser, *High Energy Density Phys.*, 3 (2007) 115-119.

[12] H. Nishimura, R. Mishra, S. Ohshima, H. Nakamura, M. Tanabe, T. Fujiwara, N. Yamamoto, S. Fujioka, D. Batani, M. Veltcheva, T. Desai, R. Jafer, T. Kawamura, Y. Sentoku, R. Mancini, P. Hakel, F. Koike, and K. Mima, Energy transport and isochoric heating of a low-Z, reduced-mass target irradiated with a high intensity laser pulse, *Phys. Plasmas*, 18 (2011) 022702-1-9.

[13] C. R. D. Brown, D. J. Hoarty, S. F. James, D. Swatton, S. J. Hughes, J. W. Morton, T. M. Guymer, M. P. Hill, D. A. Chapman, J. E. Andrew, A. J. Comley, R. Shepherd, J. Dunn, H. Chen, M. Schneider, G. Brown, P. Beiersdorfer, and J. Emig, Measurements of electron transport in foils irradiated with a picosecond time scale laser pulse, *Phys. Rev. Lett.*, 106 (2011) 185003.

[14] S. C. Wilks, W. L. Kruer, M. Tabak, and A. B. Langdon, Absorption of ultra-intense laser pulses, *Phys. Rev. Lett.*, 69 (1992) 1383.

[15] Y. Ping, R. Shepherd, B. F. Lasinski, M. Tabak, H. Chen, H. K. Chung, K. B. Fournier, S. B. Hansen, A. Kemp, D. A. Liedahl, K. Widmann, S. C. Wilks, W. Rozmus, and M. Sherlock, Absorption of short laser pulses on solid targets in the ultrarelativistic regime, *Phys. Rev. Lett.*, 100 (2008) 085004-1-4.

[16] F. N. Beg, A. R. Bell, A. E. Dangor, C. N. Danson, A. P. Fews, M. E. Glinsky, B. A. Hammel, P. Lee, P. A. Norreys, and M. Tatarakis, A study of picosecond laser–solid interactions up to  $10^{19}$  W cm<sup>2</sup>, *Phys. Plasmas*, 4 (1997), 447.

[17] S. J. Davidson, K. Nazir, S. J. Rose, R. Smith, G. J. Tallents, Short-pulse laser opacity measurements, *J. Quant. Spectrosc. Radiat. Transfer* 65 (2000) 151-160.

[18] S. J. Rose, Set the controls for the heart of the Sun, *Contemp. Phys.*, 45 (2004) 109-121.

[19] D. J. Hoarty, S. F. James, C. R. D. Brown, B. M. Williams, T. Guymer, M. Hill, J. Morton, D. Chapman, R. Shepherd, J. Dunn, G. Brown, M. Schneider, P. Beiersdorfer, H.

K. Chung, J. W. O. Harris, L. Upcraft, C. C. Smith and R. W. Lee, High temperature, high density opacity measurements using short pulse lasers, *J. Phys: Conf. Series*, 244 (2010) 012002-1-6.

[20] G. B. Zimmerman and W. L. Kruer, "Numerical simulation of laser-initiated fusion." *Comments Plasma Phys. Controlled Fusion* 2 (1975) 51.

[21] J. A. Harte, W. E. Alley, D. S. Bailey, J. L. Eddleman, and G. B. Zimmerman, LASNEX—A 2-D physics code for modeling ICF, in *Inertial confinement fusion 1996 ICF annual report*, UCRL-LR-105821-96, eds. J. Carpenter and D. Correll, 1997, pp. 150-164. (available at [https://lasers.llnl.gov/multimedia/publications/icf\\_reports/](https://lasers.llnl.gov/multimedia/publications/icf_reports/))

[22] D. S. Kershaw, Interaction of relativistic electron beams with high Z plasmas, Report UCRL-77045 (1975) and D. S. Kershaw, Computer simulation of superthermal transport for laser fusion, UCRL-83494 (1979). (Both available at the DOE Office of Science and Technical Information, [www.osti.gov](http://www.osti.gov))

[23] E. E. Fill, Ultrashort-pulse laser plasmas: Fraction of hot electrons escaping from the target and electron spectra in planar and spherical geometry, *Phys. Plasmas*, 12 (2005), 052704-1-7.

[24] J. Myatt, W. Theobald, J. A. Delettrez, C. Stoeckl, M. Storm, T. C. Sangster, A. V. Maximov, and R. W. Short, High-intensity laser interactions with mass-limited solid targets and implications for fast-ignition experiments on OMEGA EP, *Phys. Plasmas*, 14 (2007) 056301-1-8.

[25] T. Tanimoto, H. Habara, R. Kodama, M. Nakatsutsumi, Kazuo A. Tanaka, K. L. Lancaster, J. S. Green, R. H. H. Scott, M. Sherlock, Peter A. Norreys, R. G. Evans, M. G. Haines, S. Kar, M. Zepf, J. King, T. Ma, M. S. Wei, T. Yabuuchi, F. N. Beg, M. H. Key, P. Nilson, R. B. Stephens, H. Azechi, K. Nagai, T. Norimatsu, K. Takeda, J. Valente, and J. R. Davies, Measurements of fast electron scaling generated by petawatt laser systems, *Phys. Plasmas*, 16 (2009) 062703-1-6.

[26] J. N. Bahcall, A. M. Serenelli, and S. Basu, New solar opacities, abundances, helioseismology, and neutrino fluxes, *Ap. J. Lett.*, 621 (2005) L621. see the standard solar model (BS2005-OP): <http://www.sns.ias.edu/~jnb/>

[27] S. Basu and H. M. Antia, Helioseismology and solar abundances, *Physics Reports*, 457 (2008) 217-283.

[28] S. Turck-Chièze, G. Loisel, D. Gilles, L. Piau, C. Blancard, T. Blenski, M. Busquet, T. Caillaud, P. Cossé, F. Delahaye, G. Faussurier, J. Fariaut, F. Gilleron, J.A. Guzik, J. Harris, D.P. Kilcrease, N.H. Magee, J.C. Pain, Q. Porcherot, M. Poirier, G. Soullier, C.J. Zeppen, S. Bastiani-Ceccotti, C. Reverdin, V. Silvert, F. Thais, B. Villette, Radiative properties of stellar plasmas and open challenges, *Astrophys. Space Sci.*, 336 (2011)103–109.

[29] P. A. Keiter, K. Mussack, S. R. Klein, An experimental concept to measure opacities under solar-relevant conditions, *High Energy Density Phys.*, 9 (2013) 319-324.

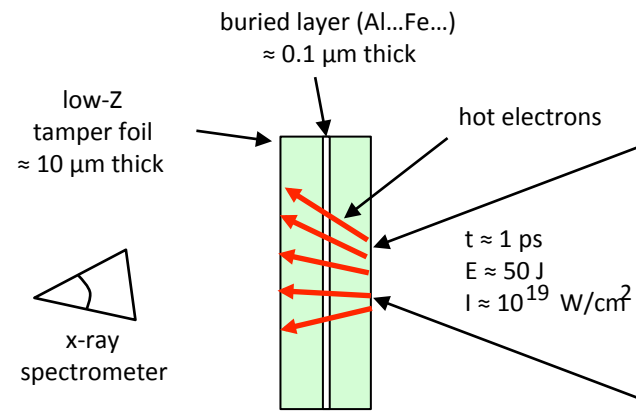
[30] Y. T. Lee, A model for ionization balance and L-shell spectroscopy of non-LTE plasmas, *J. Quant. Spectrosc. Radiat. Transfer* (1987) 131–145.

[31] H. A. Scott and S. B. Hansen, Advances in NLTE modeling for integrated simulations, *High Energy Density Phys.*, 6 (2010) 39–47.

## Figure Captions

1. Short pulse heated target. A short laser pulse, incident from the right, creates hot electrons, which heat a thin, layered target. An x-ray spectrometer records the emission, from which the opacity of the buried layer is determined.
2. Space-time plot of plasma variables for a CH/Al/CH target. The laser hits the right side of the target and the hot electron energy is input in a thin region. The hot electron source has an intensity of  $3.8 \times 10^{17}$  W/cm<sup>2</sup>, a pulse length of 0.5 ps and a temperature of 300 keV. The target is 8 μm thick, with a 0.15-μm-thick Al layer placed 6 μm from the front surface. Panel (a) shows the temperature, while panel (b) shows the density. The color scale for both variables is presented in the middle of the figure.
3. Density and temperature history of the Al layer. The target and laser parameters are the same as for Figure 2. A period of nearly constant conditions is indicated by the box.
4. Density and temperature histories of Al layer with different tamper materials. The layer is placed at the center of the target. Panel (a) shows the density for CH, amorphous carbon (aC) and diamond tampers, as indicated, while panel (b) shows the temperature. The target thicknesses are chosen to maintain the same mass column density as the tamper density is varied.
5. Density and temperature profiles for long pulse compressed target. The target is a 14-μm-thick diamond foil with a 0.15 μm Al-layer placed 4-μm from the right side. The long pulse laser irradiates the left side and the short-pulse laser hits the right side. Panel (a) shows density profiles at various times ranging from 20 to 200 ps. Panel (b) shows the temperature. A shock wave created by the ablation pressure of the long pulse propagates through the target, passing the layer at approximately 180 ps. The short pulse laser is then fired, heating the compressed target.
6. Electron density/temperature profile of the sun. The surface is at the lower left, while the center is at the upper right. The vertical line marks the radiative/convective boundary. The main region of interest for opacity measurements is in the upper part of the radiative region as indicated. The data are from the standard solar model of ref. [26].
7. Electron density and temperature history of Fe layer. The targets comprise a 9-μm-thick CH foil with Fe or Fe/CH layers in the center. Panels (a) shows the electron density and vs. time for 3 different Fe concentrations as labeled, while panel (b) shows the electron temperature.
8. Emitted specific intensity of a buried Fe layer target. The target comprises a 9-μm thick CH foil with a 0.1 μm Fe layer in the center. The emission is presented at 5 ps.

Figure 1



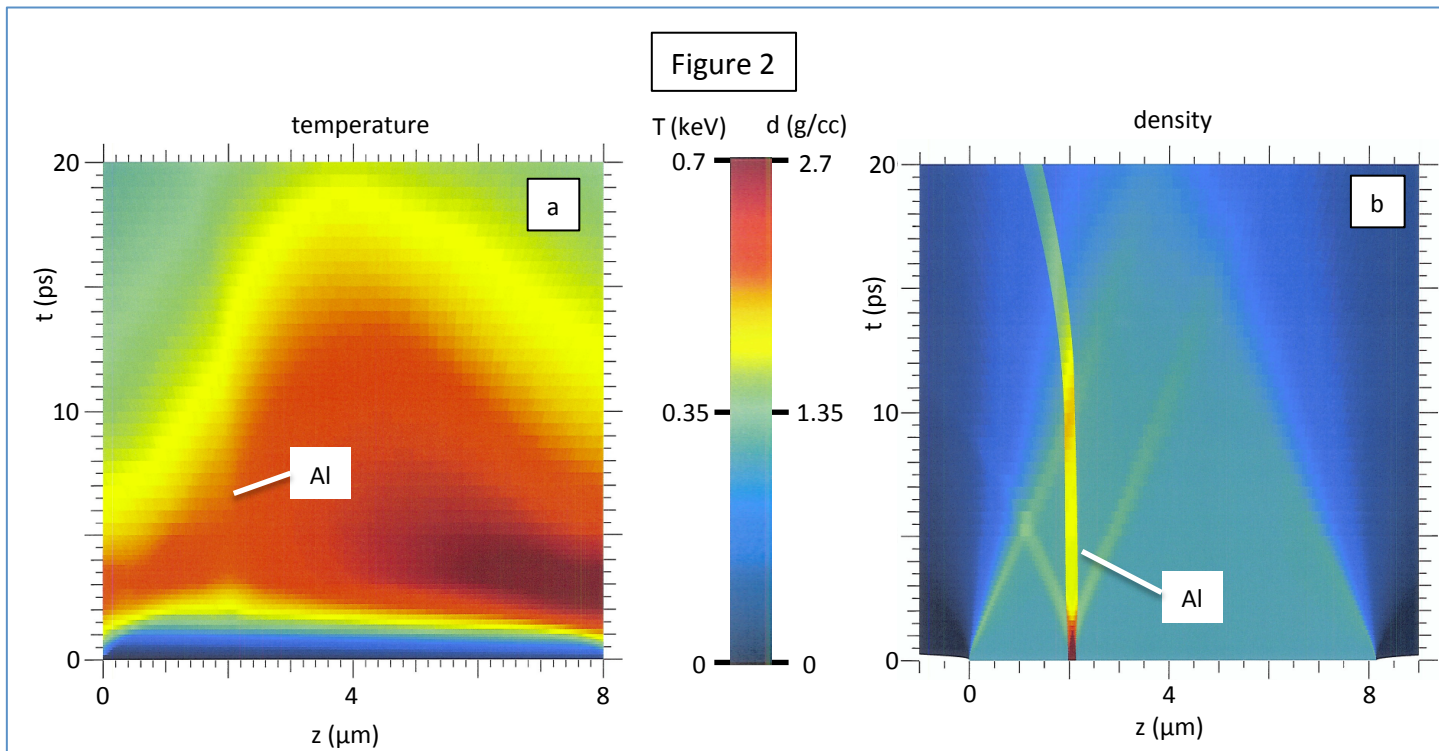


Figure 3

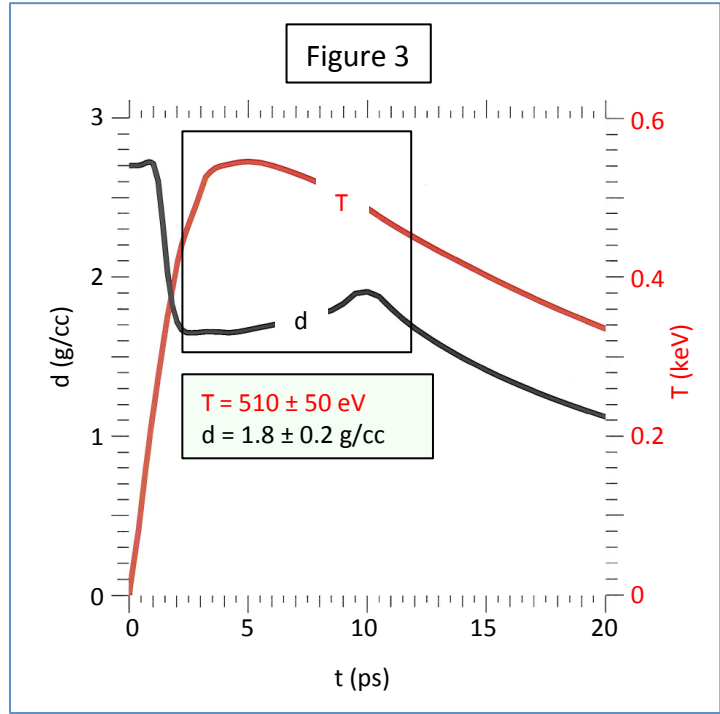


Figure 4

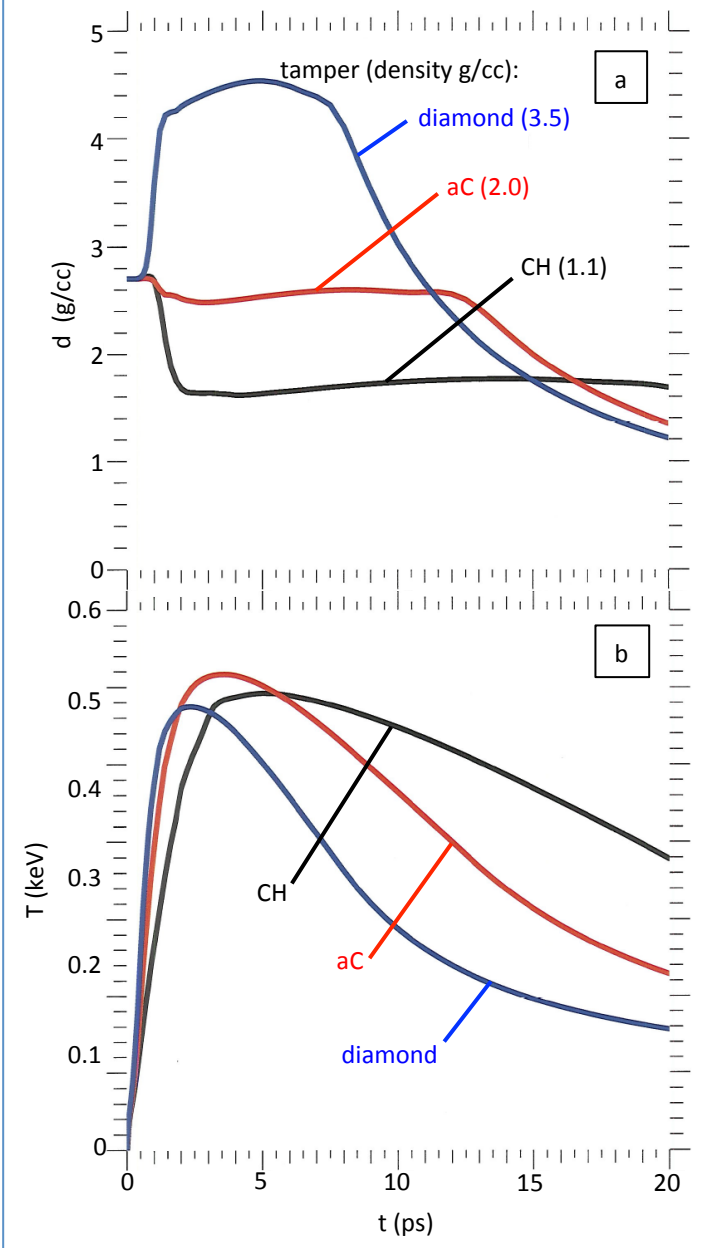


Figure 5

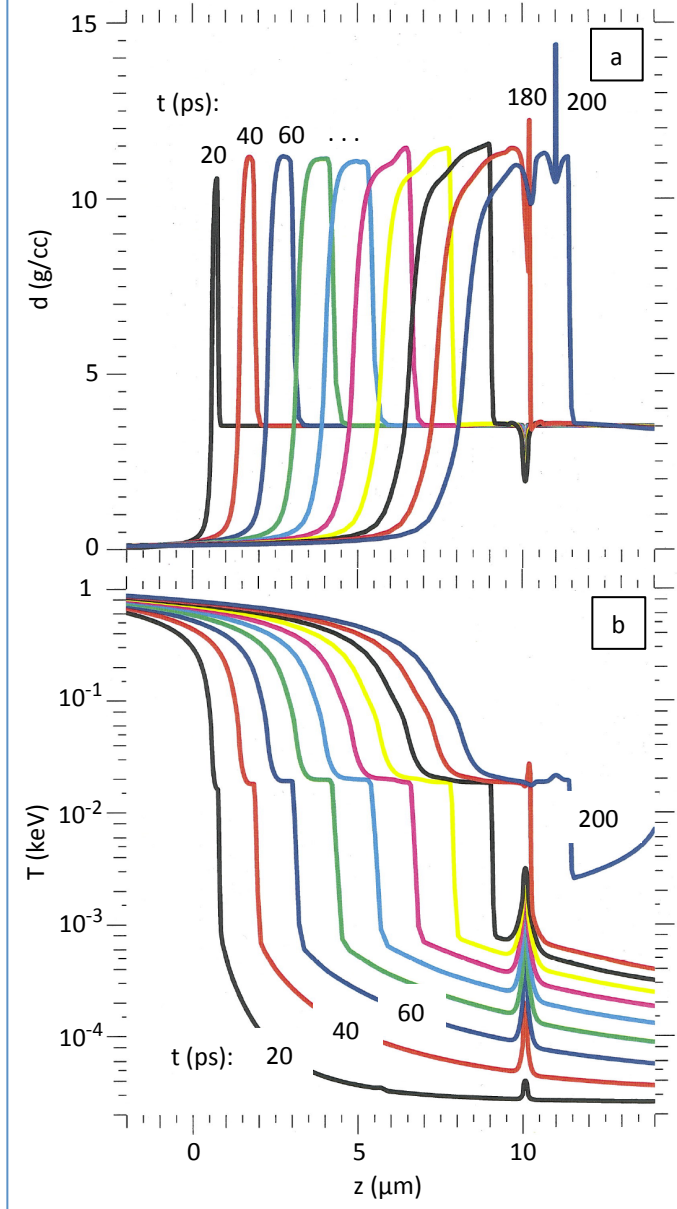


Figure 6

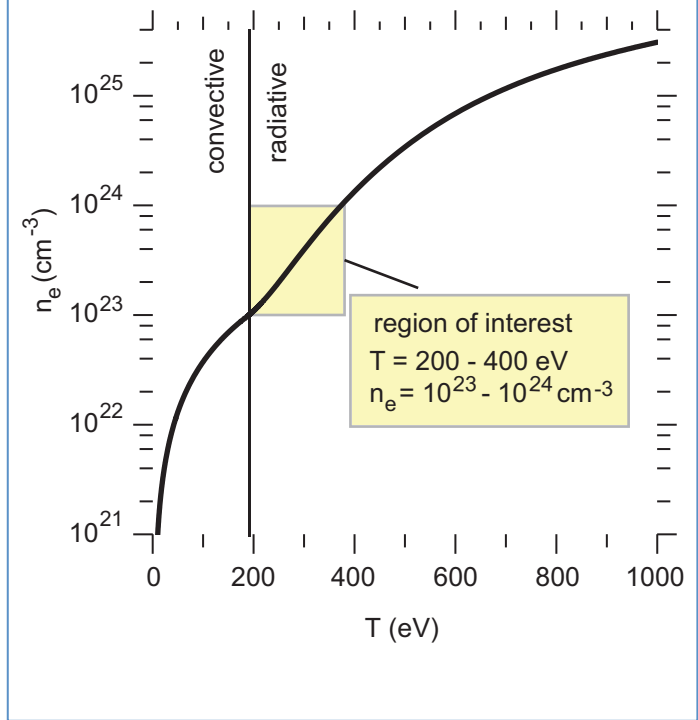


Figure 7

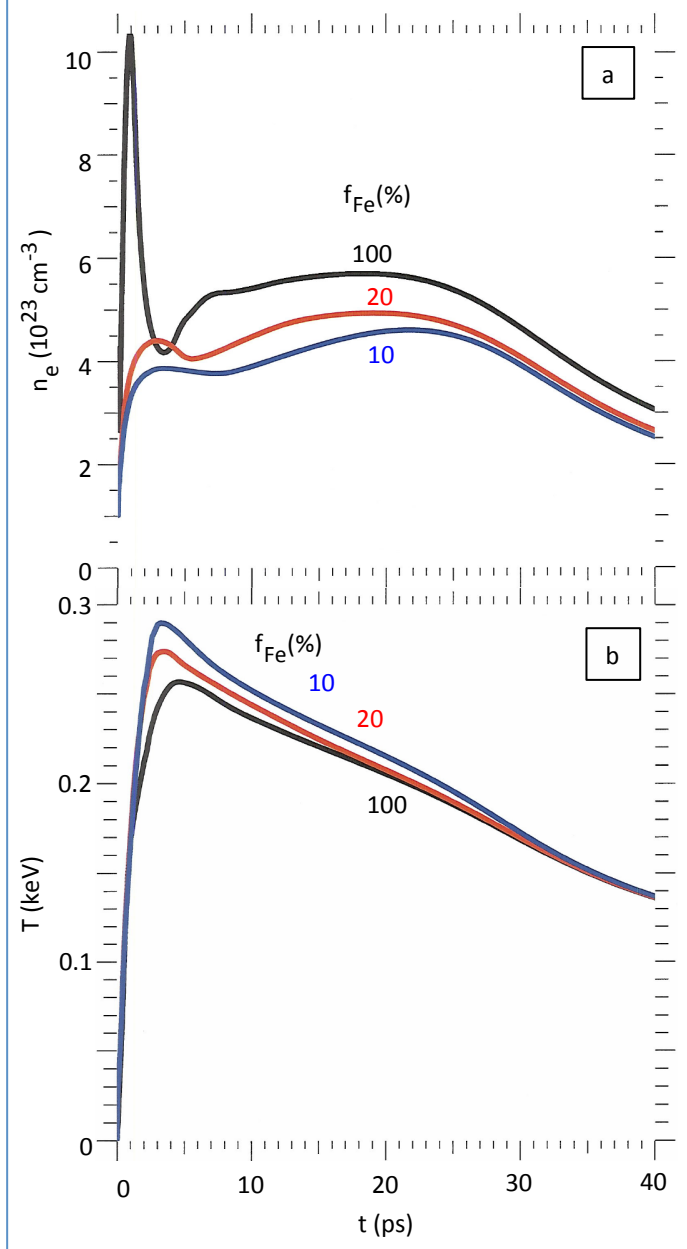


Figure 8

